NANO LETTERS

pubs.acs.org/NanoLett

The Resonant Body Transistor

Dana Weinstein,*[,†] and Sunil A. Bhave

Cornell University, 405 Phillips Hall, Ithaca, New York 14853

ABSTRACT This paper introduces the resonant body transistor (RBT), a silicon-based dielectrically transduced nanoelectromechanical (NEM) resonator embedding a sense transistor directly into the resonator body. Combining the benefits of FET sensing with the frequency scaling capabilities and high quality factors (*Q*) of internal dielectrically transduced bar resonators, the resonant body transistor achieves >10 GHz frequencies and can be integrated into a standard CMOS process for on-chip clock generation, high-*Q* microwave circuits, fundamental quantum-state preparation and observation, and high-sensitivity measurements. An 11.7 GHz bulk-mode RBT is demonstrated with a quality factor *Q* of 1830, marking the highest frequency acoustic resonance measured to date on a silicon wafer.

KEYWORDS MEMS, NEMS, resonator, transistor, FET sensing, piezoresistance

In recent years, nanomechanical resonators have been implemented for quantum-state preparation and observation in macroscopic objects. Such experiments include measurements near the ground state of motion,[1,2] nanomechanical squeezing,[3] and quantum mechanical entanglement.[4] Nanoscale resonators are also being developed to enhance measurement sensitivity toward the goal of single-molecule mass spectrometry.[5] Resonators employed within all these areas of research have achieved frequencies in the kilohertz to megahertz range. Nanoelectromechanical (NEM) resonators operating at multi-GHz frequencies would increase measurement sensitivity and provide quantum mechanical cooling, squeezing, and entanglement at higher, more accessible temperatures. However, the fundamental obstacle of scaling NEM resonators to multi-GHz frequencies is the need for a sense transducer that overcomes capacitive and parasitic feed-through and provides adequate sensitivity to measure mechanical motion at those frequencies. The resonant body transistor (RBT) presented in this work surmounts this challenge by integrating a sense transistor directly into the resonant body of a dielectrically transduced NEM resonator.

The authors have previously demonstrated longitudinal bar resonators in silicon using a novel method to drive and sense acoustic waves in the bar.[6] This mechanism, termed "internal dielectric transduction", incorporates thin dielectric film transducers inside the resonator body for electrostatic (capacitive) transduction. Internal dielectrically transduced resonators have yielded the highest acoustic resonance frequencies (up to 6.2 GHz) and highest frequency-quality factor products ($f.Q$ up to 5.1×10^{13}) published to date in silicon. Moreover, these dielectrically transduced resonators demonstrate improved efficiency as resonance frequency increases, providing a means of scaling NEM resonators to previously unattainable frequencies. However, at multigigahertz frequencies, capacitive feed-through becomes significant and prevents capacitive detection of NEM resonance without three-port mixing measurements that require an external frequency source impractical for integrated applications.

The concept of using field effect transistors (FETs) for sensing mechanical motion while overcoming capacitive feed-through has been around since the advent of microelectromechanical systems. In 1967, Nathanson et al. demonstrated the resonant gate transistor (RGT), driving resonance in a conductive cantilever with an air-gap capacitive electrode.[7] The RGT cantilever functions as the gate of an air-gap transistor with output drain current modulated by the cantilever resonant motion.

More recently, FET sensing has been implemented in a variety of micromechanical devices. Resonant gate transistors similar to Nathanson's device have been demonstrated in silicon air-gap resonators up to 14 MHz.[8,9] Mechanical resonators sensed through direct elastic modulation of a transistor channel have also been demonstrated. Such devices include air gap resonators with embedded FETs up to 71 MHz,[10] mechanical mixing in single electron transistors up to 245 MHz,[11] piezoelectrically in GaN air-gap resonators up to 2 MHz.[12]

The resonant body transistor combines the benefits of FET sensing with the frequency scaling and high-*Q* capabilities of internal dielectrically transduced bar resonators. Figure 1 shows a top-view schematic of the resonant body transistor, illustrating its principle of operation. The region in light gray represents the undoped active area of the FET, while the blue region is highly doped. The active area near the drive electrode is biased into accumulation (red), so that a capacitive force acts across the thin dielectric film (yellow), driving longitudinal resonant motion in the freely suspended body. A gate voltage is applied to the opposing electrode,

* To whom correspondence should be addressed. E-mail: dana@mtl.mit.edu.

† This work was performed while both authors were at Cornell University. D.W. is currently an assistant professor in the Department of Electrical Engineering and Computer Science at the Massachusetts Institute of Technology.

Received for review: 11/09/2009
Published on Web: 02/24/2010

© 2010 American Chemical Society

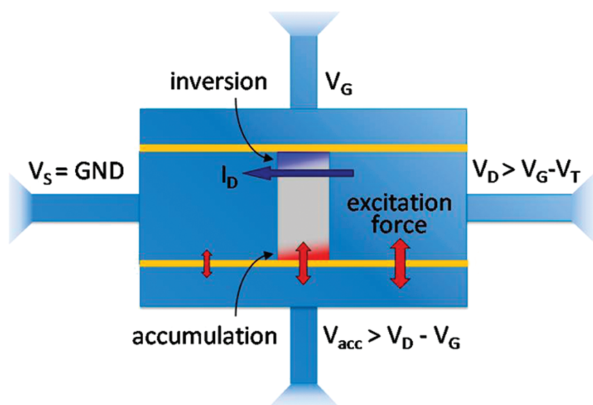

FIGURE 1. Top-view schematic showing principle of operation of a bulk-mode dielectrically transduced resonant body transistor. The RBT geometry is similar to that of an Independent-Gate FinFET with two independent gates. One gate biases the active region of the FET (gray) into accumulation to generate an electrostatic force to drive longitudinal (bulk) acoustic waves in the resonator. The other gate is biased in inversion, generating a current between source and drain. Elastic waves in the resonator piezoresistively modulate the drain current, enabling electrical pick-off of acoustic resonance at multi-GHz frequencies.

generating an inversion channel (blue) that results in a DC drain current. At resonance, elastic waves formed in the resonator modulate the drain current both by physically changing the gate capacitance and by piezoresistive modulation of carrier mobility. The latter of these effects dominates the output signal.

Using internal dielectric transduction to drive and sense acoustic resonance,[6] the amplitude of vibrations at resonance is given by

$$U_0|_{\text{cap}} = \frac{4Q\varepsilon V_{\text{DC}} v_{\text{in}}}{n^2\pi^2 Y}\frac{L}{g^2}\sin\left(\frac{k_n g}{2}\right) \qquad (1)$$

where g is the dielectric thickness, L is the length of the resonator, ε_f is the dielectric permittivity, V_{DC} is the bias voltage across the dielectric films, v_{in} is the AC excitation voltage, Y is the Young's modulus, n is the harmonic of resonance, and k_n is the wavenumber. With the bias restrictions of Figure 1, the amplitude of vibrations in the RBT is

$$U_0|_{\text{RBT}} = \frac{U_0|_{\text{cap}}}{V_{\text{DC}}W}\left[\left(\frac{W}{2} - \frac{L_{\text{gate}}}{2}\right)(V_D - V_{\text{acc}}) - \left(\frac{W}{2} - \frac{L_{\text{gate}}}{2}\right)V_{\text{acc}} + \frac{L_{\text{gate}}}{2}(V_D - V_{\text{acc}})\right] \qquad (2)$$

Here, W is the width of the resonator and L_{gate} is the transistor gate length. The strain induced in the resonator piezoresistively modulates the drain current running through the inversion layer. Assuming a piezoresistive coefficient of π_{110}, the piezoresistive modulation of the FET drain current I_D is

$$i_{\text{out}}|_{\text{RBT}} \approx I_D\frac{d\mu_n}{\mu_n} = I_D\pi_{110}Yk_nU_0|_{\text{RBT}}\cos\left(\frac{k_n g}{2}\right) \qquad (3)$$

The motional impedance $R_x \equiv v_{in}/i_{out}$ for a capacitive resonator and RBT of identical geometry is shown for comparison in Figure 2.

RBTs were fabricated side-by-side with independent-gate FinFETs[13] at the Cornell Nanoscale Facility (CNF). Scanning electron micrographs (SEMs) of a FinFET and 12 GHz RBT are shown in Figure 3. The devices were tested in a two-port configuration at room temperature in a vacuum probe station, as illustrated in Figure 4. The devices were tested in vacuum to prevent ionization of air in the fringe fields near the dielectric, where 5 V were applied across a 15 nm gap. The vacuum also prevented adsorption of molecules onto the surface of the resonator over time, which can

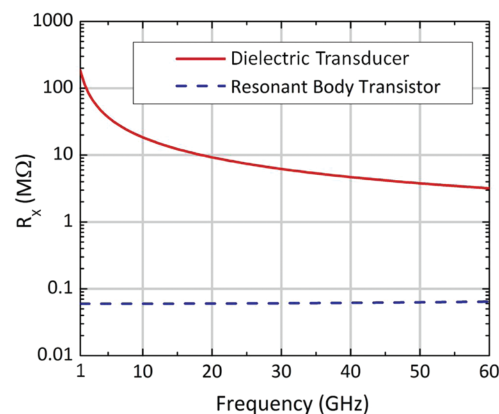

FIGURE 2. Comparison of motional impedance $R_x \equiv v_{in}/i_{out}$ of a capacitively transduced bar resonator and an RBT with identical geometry. The third harmonic of longitudinal vibrations is assumed with a 15 nm silicon nitride dielectric transducer. W = 500 nm, device thickness is 220 nm, and gate voltage is 5 V. Quality factor of resonance is taken to scale as $Q = (2 \times 10^{13})/f$. The RBT shows more than order-of-magnitude higher transduction efficiency (lower R_x) over a broad range of frequencies above 1 GHz.

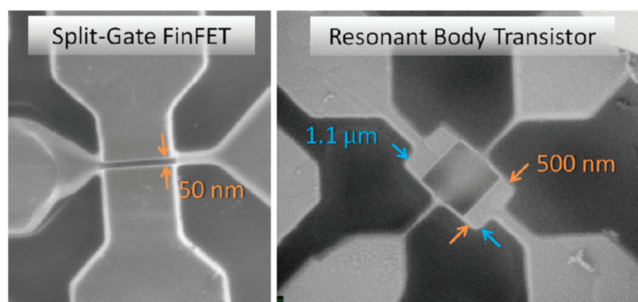

FIGURE 3. Scanning electron micrographs of an Independent-Gate FinFET (left) and 12 GHz RBT (right). Both devices were fabricated side-by-side in the same process. Gate length of both FinFET and RBT are 500 nm. Fin width of the FinFET is 50 nm. Source and drain routing beams for the RBT are only 30 nm wide, contributing significant series resistance to device characteristics. Both FinFET and RBT are released in a hydrofluoric acid timed wet etch and freely suspended.

© 2010 American Chemical Society

DOI: 10.1021/nl9037517 | Nano Lett. 2010, 10, 1234--1237

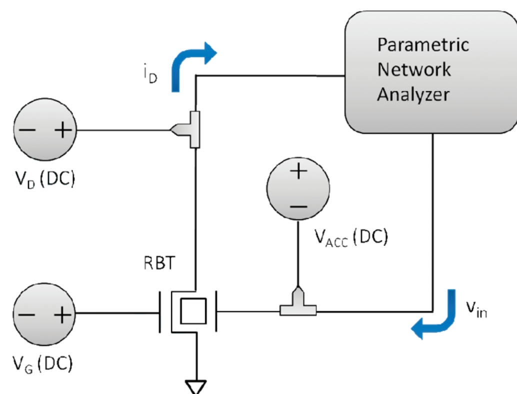

FIGURE 4. Schematic of two-port measurement for frequency characterization of RBT. The drive and sense gates of the RBT were biased into accumulation and inversion, respectively. An AC excitation was superimposed on the drive gate using a parametric network analyzer. Measurements were done under vacuum to prevent both arching across dielectric transducer edges and molecular adsorption on the RBT surface.

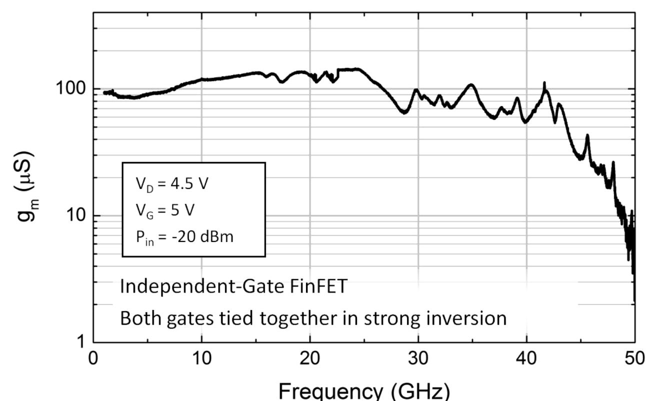

FIGURE 5. De-embedded frequency response of a freely suspended independent-gate FinFET with both gates tied together and biased into strong inversion. This biasing scheme provides electrical frequency characterization of the transistor. Fin width = 50 nm and gate length = 500 nm.

degrade the quality factor. After de-embedding the device from the probe pads and routing, the transconductance is obtained from the Y-parameters, $g_m = Y_{21} - Y_{12}$, as in the case of conventional transistor measurements.

To test the performance of the transistor sensing in the RBT, an independent-gate FinFET was first measured tying both gates together and biasing the device at $V_G = 5$ V into strong inversion. The resulting frequency response of the FinFET is presented in Figure 5. The FinFET tested has a fin width of 50 nm and a gate length of $L_{gate} = 500$ nm. The transconductance of the FinFET begins to drop around 42 GHz, corresponding the frequency limit of the transistor.

The RBTs were then tested in the configuration outlined in Figures 1 and 4. The de-embedded frequency response of an 11.7 GHz RBT is shown in Figure 6. The electromechanical Q of the RBT is 1831, resulting in an $f.Q$ product of 2.1×10^{13}. The device exhibits a clear signal of over 13 μS (piezoresistive transconductance) above the background

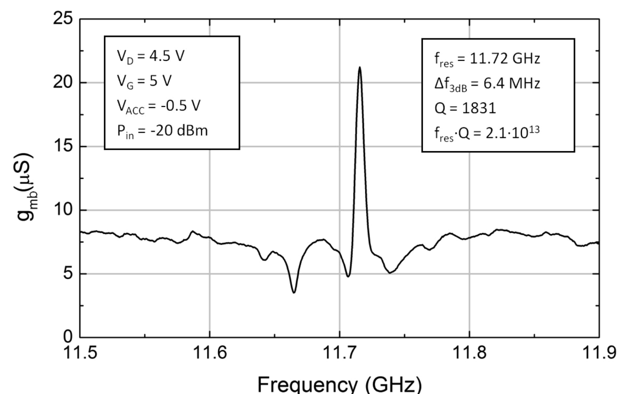

FIGURE 6. De-embedded frequency response of a resonant body transistor. The biasing scheme for the RBT is as shown in Figure 4. An off-resonance signal floor of 7 μS is associated with a direct electrical modulation of the drain channel through the drive gate (back-gate transconductance g_{mb}). The third harmonic resonance frequency of 11.7 GHz, with electromechanical Q of 1831 and piezoresistive transconductance of 22 μS, is the highest frequency electrically measured to date in silicon.

signal, and can be improved further by reducing the series resistance of the suspension beams to the resonant bar and reducing the FET gate length. As seen in Figure 3, the source and drain of the RBT are ~30 nm wide, resulting in a non-negligible series resistance which adversely affects the transconductance and quality factor of the device.

The 11.7 GHz resonance of the RBT presented in this work is the highest acoustic frequency measured electrically in a silicon resonator to date. This first demonstration of a resonant body transistor using internal dielectric drive and FET sensing promises the scaling nanofabricated resonators to multigigahertz frequencies. The RBT was fabricated side-by-side with independent-gate FinFETs, indicating the capacity of these resonators for CMOS integration at front end-of-line fabrication. Such a hybrid NEMS-CMOS technology will provide RF CMOS circuit designers with high-Q active devices operating up to 60 GHz and beyond and will enable us to bring quantum electromechanical systems out of dilution refrigerators and into accessible benchtop experiments.

Acknowledgment. This research was supported by the National Defense Science and Engineering Grant, Lockheed Martin, and Army Research Laboratories. Nanofabrication of the RBT was performed at the Cornell Nanoscale Facility, a member of the National Nanotechnology Infrastructure Network.

Supporting Information Available. Additional information is available outlining the de-embedding process necessary for RF measurement of a single probed device. This material is available free of charge via the Internet at http://pubs.acs.org.

REFERENCES AND NOTES

(1) LaHaye, M. D.; Buu, O.; Camarota, B.; Schwab, K. C. *Science* **2004**, *304* (5667), 74–77.
(2) Schliesser, A.; Arcizet, O.; Riviere, R.; Anetsberger, G.; Kippenberg, T. J. *Nat. Phys.* **2009**, *5*, 509–514.
(3) Woolley, M. J.; Doherty, A. C.; Milburn, G. J.; Schwab, K. C. *Phys. Rev. A* **2008**, *78* (6), No. 062303.

© 2010 American Chemical Society

DOI: 10.1021/nl9037517 | *Nano Lett.* **2010,** *10,* 1234--1237

(4) LaHaye, M. D.; Suh, J.; Echternach, P. M.; Schwab, K. C.; Roukes, M. L. *Nature* **2009**, *459*, 960–964.
(5) Naik, A. K.; Hanay, M. S.; Hiebert, W. K.; Feng, X. L.; Roukes, M. L. *Nat. Nanotechnol.* **2009**, *4*, 445–449.
(6) Weinstein, D.; Bhave, S. A. *IEEE Int. Electron Device Meet.* **2007**, 415–418.
(7) Nathanson, H. C.; Newell, W. E.; Wickstrom, R. A.; Davis, J. R., Jr. *IEEE Trans. Electron Devices* **1967**, *14* (3), 117–133.
(8) Durand, C.; Casset, F.; Renaux, P.; Abele, N.; Legrand, B.; Renaud, D.; Ollier, E.; Ancey, P.; Ionescu, A. M.; Buchaillot, L. *Electron Device Lett.* **2008**, *29* (5), 494–496.
(9) Colinet, E.; Durand, C.; Duraffourg, L.; Audebert, P.; Dumas, G.; Casset, F.; Ollier, E.; Ancey, P.; Carpentier, J.-F.; Buchaillot, L.; Ionescu, A. M. *J. Solid-State Circuits* 2009*44* (1), 247–257.
(10) Grogg, D.; Mazza, M.; Tsamados, D.; Ionescu, A. M. *IEEE Int. Electron Device Meet.* **2008**, 1–4.
(11) Kim, H. S.; Qin, H.; Blick, R. H. *Appl. Phys. Lett.* **2007**, *91*, 143101.
(12) Faucher, M.; Grimbert, B.; Cordier, Y.; Baron, N.; Wilk, A.; Lahreche, H.; Bove, P.; François, M.; Tilmant, P.; Gehin, T.; Legrand, C.; Werquin, M.; Buchaillot, L.; Gaquière, C.; Théron, D. *Appl. Phys. Lett.* **2009**, *94*, 233506.
(13) Huang, X.; Lee, W.-C.; Kuo, C.; Hisamoto, D.; Chang, L.; Kedzierski, J.; Anderson, E.; Takeuchi, H.; Choi, Y.-K.; Asano, K.; Subramanian, V.; King, T.-J.; Bokor, J.; Hu, C. *IEEE Int. Electron Device Meet.* **1999**, 67–70.

© 2010 American Chemical Society

The Resonant Body Transistor

Supporting Information

De-embedding procedure for RBT measurement

Detection of the RBT and Split-Gate FinFET requires high-frequency measurement ranging over tens of GHz. However, to probe each resonator and Fin-FET individually, large probe pads and routing to each device result in significant capacitance which dominates the measured signal. The parasitic capacitance and inductance of the probe pads and routing can be subtracted from the measured device using de-embedding structures on-chip. Models of the de-embedding structures used for the RBT and FinFET measurements are shown in Figure S1. Finite Element Analysis (FEA) on these models in Ansoft HFSS in combination with the de-embedding method presented here result in a lowering of the capacitive floor well below the expected device signal.

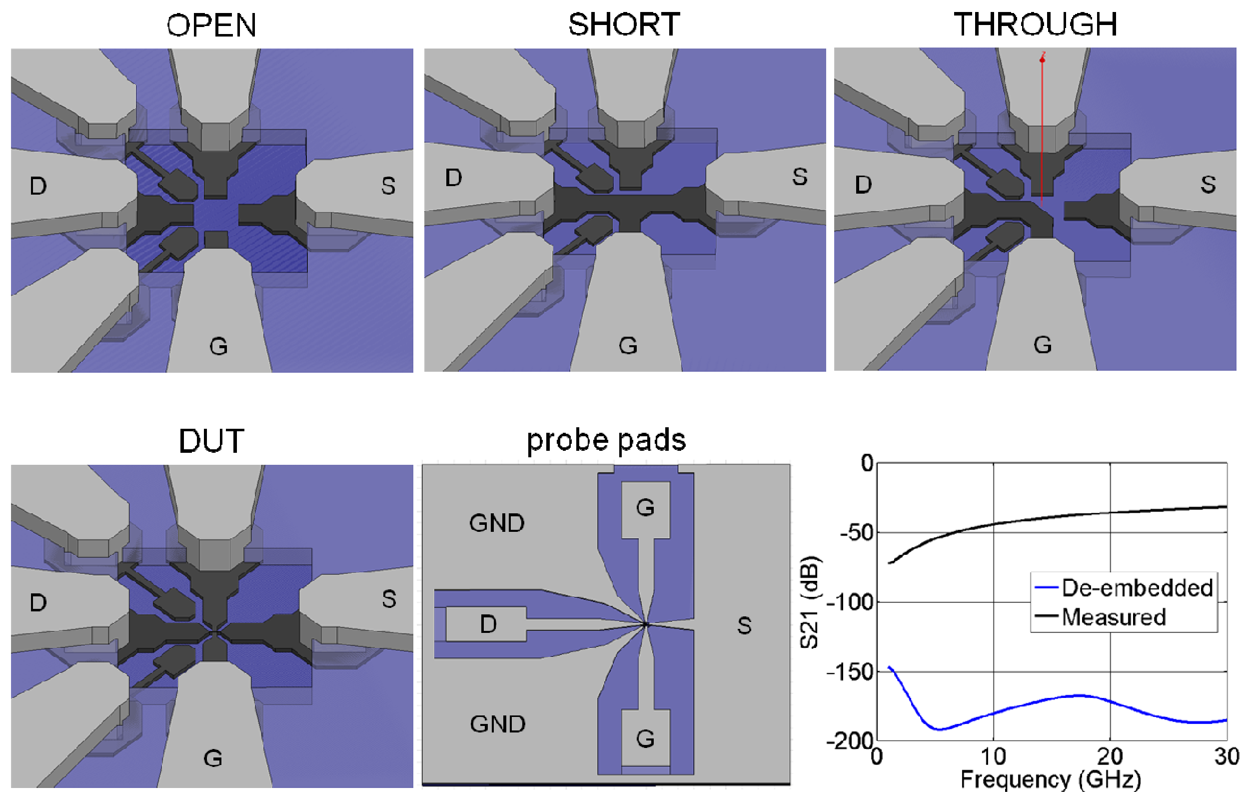

Figure S1. De-embedding structures fabricated on-chip to subtract parasitic capacitance and inductance of the probe pads and routing, lowering the measurement floor.

The de-embedding algorithm implemented in these measurements was developed by Cho *et al*[S1], and is outlined below.

1. Measure S-parameters of the device under test (DUT), open, short, and through structures $[S^{DUT}]$, $[S^{OPEN}]$, $[S^{SHORT}]$, $[S^{THRU}]$.

2. Convert $[S^{OPEN}] \rightarrow [Y^{OPEN}]$, $[S^{SHORT}] \rightarrow [Y^{SHORT}]$.

3. Subtract $[Y^{S-O}] = [Y^{SHORT} - Y^{OPEN}]$.

4. Convert $[Y^{S-O}] \rightarrow [Z^{S-O}]$.

5. Calculate ABCD matrices of the input and output pads (PAD1 and PAD2, respectively) to the device:

$$[A^{PAD1}] = \begin{bmatrix} 1 & Z_{PAD} \\ Y_{PAD} & 1 + Y_{PAD}Z_{PAD} \end{bmatrix}$$

$$[A^{PAD2}] = \begin{bmatrix} 1 + Y_{PAD}Z_{PAD} & Z_{PAD} \\ Y_{PAD} & 1 \end{bmatrix}$$

where $Y_{PAD} = Y_{11}^{OPEN} + Y_{12}^{OPEN}$ and $Z_{PAD} = Z_{11}^{S-O} - Z_{12}^{S-O}$.

6. Convert $[S^{THRU}] \rightarrow [A^{THRU}]$.

7. Calculate

$$[A^{INT}] = [A^{PAD1}]^{-1}[A^{THRU}][A^{PAD2}]^{-1}$$

$$[A^{INT}] \rightarrow [S^{INT}]$$

$$Z_C \equiv \pm Z_0 \sqrt{\frac{(1 + S_{11}^{INT})^2 - (S_{21}^{INT})^2}{(1 - S_{11}^{INT})^2 - (S_{21}^{INT})^2}}$$

$$\gamma = -\frac{1}{\ell} ln\left[\left(\frac{1 - (S_{11}^{INT})^2 + (S_{21}^{INT})^2}{2S_{21}^{INT}} \pm \kappa\right)^{-1}\right]$$

$$\kappa = \sqrt{\frac{(1 - (S_{21}^{INT})^2 + (S_{11}^{INT})^2)^2 - (2S_{11}^{INT})^2}{(2S_{21}^{INT})^2}}$$

8. Calculate ABCD matrices $[A^{INT1}]$, $[A^{INT2}]$ using input and output interconnect lengths ℓ_1, ℓ_2.

$$\begin{bmatrix} A & B \\ C & D \end{bmatrix} = \begin{bmatrix} cosh(\gamma\ell) & Z_C sinh(\gamma\ell) \\ \frac{1}{Z_C} sinh(\gamma\ell) & cosh(\gamma\ell) \end{bmatrix}$$

9. Calculate

$$[A^{IN}] = [A^{PAD1}][A^{INT1}]$$

$$[A^{OUT}] = [A^{INT2}][A^{PAD2}]$$

10. Convert $[S^{DUT}] \rightarrow [A^{DUT}]$.

11. Calculate $[A^{D}] = [A^{IN}]^{-1}[A^{DUT}][A^{OUT}]^{-1}$

12. Convert $[A^{D}] \rightarrow [S^{D}]$.

The resulting $[S^{D}]$ matrix corresponds to the 2-port frequency response of the device de-embedded from the probe pads and routing. It should be noted that de-embedding using the through structure does not remove the series resistance of the suspension beams to the RBT or the FinFET, but does eliminate the contact resistance between the metal and silicon layers.

References

[S1] Cho, M.-H.; Huang, G.-W.; Chiu, C.-S.; Chen, K.-H.; Peng, A.-S.; Teng, Y.-M. *IEICE Transactions on Electronics* **2005**, *E88-C* (5), 845–850.